Color Reflectance Modeling Using a Polychromatic Laser Range Sensor

Réjean Baribeau, Marc Rioux, and Guy Godin

Abstract—**This paper describes a system for simultaneously measuring the 3-D shape and color properties of objects. Range data are obtained by triangulation over large volumes of the scene, whereas color components are separated by means of a white laser. Details are given concerning the modeling and the calibration of the system for bidirectional reflectance-distribution function measurements. A reflection model is used to interpret the data collected with the system in terms of the underlying physical properties of the target. These properties are the diffuse reflectance of the body material, the Fresnel reflectance of the air-media interface, and the slope surface roughness of the interface. Experimental results are presented for the extraction of these parameters. By allowing the subtraction of highlights from color images and the compensation for surface orientation, spectral reflectance modeling can help to understand 3-D scenes. A practical example is given where a color and range image is processed to yield uniform regions according to material pigmentation.**

Index Terms—**Computer color vision, range measurements, reflection measurements, reflection model, surface roughness.**

I. Introduction

Understanding of images in terms of the physical properties of the underlying objects is an important issue in computer vision. This paper describes a method for the recovery of intrinsic color reflectance properties of objects using the data gathered with an autosynchronized laser sensor designed to provide both range and polychromatic intensity measurements. This system is currently being developed by the National Research Council of Canada for numerous applications: The documentation of museum artifacts is among them. In art conservation, curators are looking for tools to help the documentation and analysis of valuable works. Boulanger *et al.* [6] have shown the usefulness of the geometric data for recording and replication purposes. In the same context, registered color measurements add not only the possibility of graphics display of the objects but a potential for using the range sensor as an analytical instrument as well.

Range sensors based on active triangulation are available in various configurations such as plane of light, spot scanning, or pattern projection (see [4] for a thorough survey). They all operate by projecting light on the scene and observing the reflected light from a point that differs from that of emission. The angle of the returning light is measured using a photosensitive device and serves to compute Cartesian coordinates of the illuminated surface points. The amount of received light is also measured by the same device and bears strong similarity to that obtained using a conventional 2-D imaging system. The processing of this image alone is, thus, likely to encounter similar difficulties. However, if the analysis of the sensed intensity is done in connection with the range information, a much deeper understanding of the scene is possible. This is because the geometrical information can be used to compensate for effects of shading and specular reflections, allowing the recovery of some intrinsic reflectance properties of the 3-D scene.

The analysis of surfaces according to their reflectance properties is being increasingly recognized as a promising avenue in computer vision. Numerous works have been reported along these lines for the case of 2-D images. In this case, the missing information about shape is usually compensated by the availability of multiple images taken after some alteration of the lighting-observation conditions [13], [18], [26], [24]. For example, Klinker *et al.* [14] have shown that for simple scenes, surface and body reflection components could be separated using the information contained in 2-D images taken with R, G, and B filters. Their work is particularly relevant to this one, especially with regard to color space histogram interpretation. The survey of reflectance models made by Healey [10], along with their application to the understanding of 2-D scenes in terms of material composition, is also relevant.

Comparisons of methods and models used in computer vision must be done with respect to well-defined tasks. For the system presented here, the task is to assign to each surface element some precise spatial coordinates and a list of nonempirical color reflectance parameters. These are the *spectral reflectance* of the body material, the *Fresnel reflectance* of the surface material, and the *slope roughness* of the surface material. This assignation is done independently for three wavelength channels. To some extent, the method does not require objects to be of uniform material composition over large portions of the scene.

Section II presents an overview of surface reflectance nomenclature and introduces a reflectance model for which parameters can be established using the data collected by the laser sensor. Section III gives a description of the principle of the 3-D camera for range and color measurements. Section IV applies the method of reflection parameter extraction on scenes of increasing complexities.

II. Reflectance Nomenclature

The concept of *bidirectional reflectance-distribution function* (BRDF) has been proposed by Nicodemus *et al.* [19] as a unified approach to the specification of reflectance. BRDF is defined as

$$f_r(\theta_i, \phi_i; \theta_o, \phi_o) = \frac{dL_o(\theta_o, \phi_o)}{dE_i(\theta_i, \phi_i)}, \tag{1}$$

where $L_o(\theta_o, \phi_o)$ is the reflected *radiance* in some outgoing direction $\vec{\mu}_o$, and $E_i(\theta_i, \phi_i)$ is the *irradiance* of the reflecting surface from a small source in some incoming direction $\vec{\mu}_i$. Fig. 1 illustrates the geometry. In the absence of fluorescence or phosphorescence, the concept of BRDF can be applied at any number of specific radiation wavelengths λ, and the term *spectral* BRDF is used to designate the function $f_r(\theta_i, \phi_i; \theta_o, \phi_o; \lambda)$.

For an idealized perfectly diffusing white surface, which is also referred to as a Lambertian surface, the BRDF is given by

$$f_{r,\text{Lambert}} = \frac{1}{\pi}, \tag{2}$$

and is independent of wavelength and geometry. For real objects, the spectral BRDF takes the form

$$f_r = \frac{R(\theta_i, \phi_i; \theta_o, \phi_o; \lambda)}{\pi}, \tag{3}$$

where $R()$, which is the spectral *bidirectional reflectance factor* (BRDF factor), generally depends on wavelength and geometry.

For a large class of materials, the function $R()$ can, as a good approximation, be considered to be the sum of a *body* component and

Manuscript received November 15, 1990; revised February 1, 1991. This work was supported by the government of Canada under contract 36100-9-0266.

R. Baribeau is with the Centre d'Optique Photonique et Laser, Université Laval, Laval, Canada G1K 7P4.

M. Rioux and G. Godin are with the Autonomous Systems Laboratory, Institute for Information Technology, National Research Council, Ottawa, Canada K1A 0R6.

IEEE Log Number 9102688.

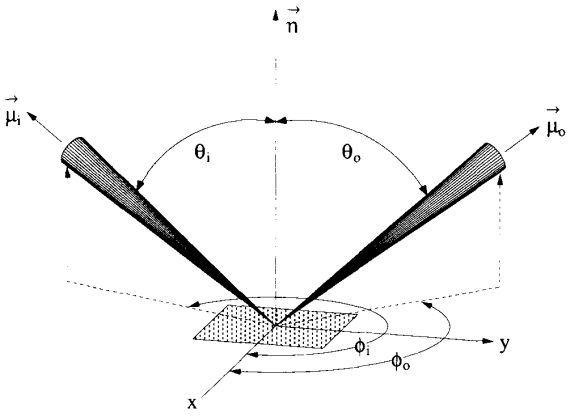

Fig. 1. Geometry of reflectance (redrawn from Nicodemus *et al.* [23]).

a *surface* component. Moreover, the geometrical dependency and the wavelength dependency of these components can be expressed as a product of functions, leading to

$$R(\theta_i, \phi_i; \theta_o, \phi_o; \lambda) = m_b(\theta_i, \phi_i; \theta_o, \phi_o) c_b(\lambda) + m_s(\theta_i, \phi_i; \theta_o, \phi_o) c_s(\lambda). \quad (4)$$

This approximate model, which is known as the *dichromatic reflection model*, has been suggested by Shafer [23] and forms the basis of many algorithms for color image understanding. Its physical soundness is discussed by Healey [10] and has been experimentally tested by Lee *et al.* [15].

A main result of the present paper is that because the geometrical information is made available by the laser sensor, the functions $c_b(\lambda)$ and $c_s(\lambda)$ can be recovered. These functions are intrinsic properties of objects and are related only to their material composition. To achieve this result, some functional forms must be provided for $m_b()$ and $m_s()$, and a way must be found to turn a laser range finder into a spectral BRDF factor measuring instrument. This last issue is discussed in the following section. Specializations of the reflection model according to specific tasks are reported in Section IV.

III. Camera Description

This section addresses the problem of turning a laser range finder into a spectral BRDF factor measuring instrument. This involves three types of considerations: The orientation parameters involved in the definition of BRDF, including the sampled surface itself, must be tractable; the raw intensity signal provided by the sensor must be linked to some more precise radiometric concept; means must be provided for sensing at different wavelengths.

A. Geometric Considerations

The range sensor considered in this paper makes use of the spot scanning approach. This technique offers the advantage that only one surface element is illuminated at any given time, thus avoiding problems connected to interreflections among objects in the scene.

Fig. 2 shows the synchronized scanning geometry that makes use of a two-sides-coated scanning mirror. The first side of this mirror participates in the projection of a laser beam on the scene, whereas the second side redirects the light reflected by the object into an imaging system. The position of the image on the detector and the known angular position of the scanning mirror allow the calculation of the (x, z) coordinates of the spot on the object; this is a task that can be repeated at short time intervals (typically 50–100 μs) during

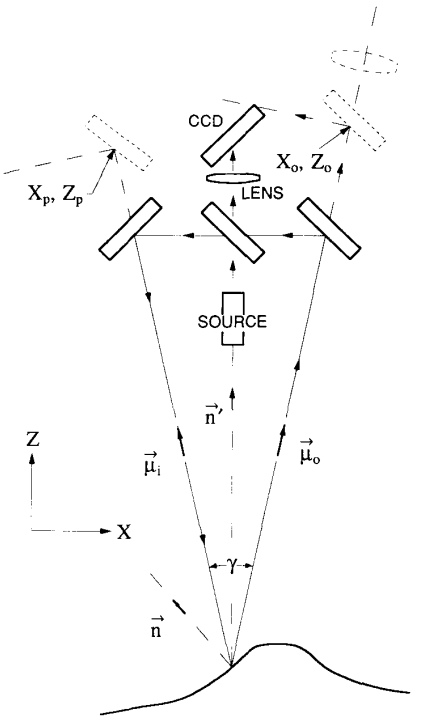

Fig. 2. Real (solid) and unfolded (dashed) geometry of the camera.

the scan . A profile obtained this way consists of a collection of coordinates (x_i, z_i) for each of the i positions of the scanning mirror. Data reduction is accomplished by interpolating this set of data for equal Δx intervals. The third coordinate y is obtained simply by mounting the whole system on a translation stage that moves in the perpendicular y direction during acquisition. A typical range image, such as the one used to synthesize the stereo pairs in the top of Fig. 5, consists of 512 × 512 values of depths z over a field of view of a few tens of centimeters in x and y and takes less than 1 min to acquire. Depth resolution is in the order of 10 μm for objects at 0.5 m from the camera and is limited mostly by speckle noise [1]. Further details concerning range acquisition can be found in previously published papers [20], [22].

One feature of the autosynchronization principle is that the *triangulation angle* γ (Fig. 2) keeps a small and almost constant value (typically 10°) over the measurement volume, thus minimizing masking and shadowing problems. The instantaneous field of view of the receiving lens also remains limited to a few degrees, regardless of the scanning angle. This fact allows negligence of foreshortening effects in the calculation of the solid angle subtended by the lens, as seen from the sampled point.

To understand how the orientations parameters $\vec{\mu}_i$, $\vec{\mu}_o$ and $\vec{n}$ can be set for any sampled point, it helps to *unfold* the geometry of the camera by replacing parts of the system by their virtual images through the fixed mirrors. In Fig. 2, one can appreciate the autosynchronization that allows the two virtual images of the scanning mirror to move synchronously. The centers of the virtual scanning mirrors (x_p, z_p) and (x_o, z_o) are seen to remain at the same positions, regardless of the scanning angle.

The position (x_p, z_p) of the *projection pivot* can be obtained through the following procedure: First, it is to be observed that if the scanning angle is kept at a fixed value and an object is moved in the

z direction, the collection of points (x_i, z_i) measured by the camera fall on a line that corresponds to one particular projection direction. Finding the intersection of two such lines, taken for extreme angles of the scanning mirror, gives (x_p, z_p) in the calibrated reference frame of the camera. The calculation requires straightforward linear regression. The procedure itself involves only the acquisition of the noninterpolated range image of a large and flat surface tilted in the y direction.

The position (x_o, z_o) of the *observation pivot* is geometrically calculated from (x_p, z_p) using the knowledge of the distance between the fixed mirrors and of the angle between them.

The coordinates of the projection and observation pivots are established once for all, and these allow the calculation of the orientation unit vectors $\vec{\mu}_i$ and $\vec{\mu}_o$ associated to any sampled point (x, y, z) on any range image.

For images that are interpolated at equal distance increments Δx and Δy, the normal $\vec{n}$ to the surface at any point is computed from the coordinates of neighboring points using the familiar derivative operators

$$\frac{1}{6\Delta x}\begin{pmatrix} -1 & 0 & 1 \\ -1 & 0 & 1 \\ -1 & 0 & 1 \end{pmatrix} \text{ and } \frac{1}{6\Delta y}\begin{pmatrix} 1 & 1 & 1 \\ 0 & 0 & 0 \\ -1 & -1 & -1 \end{pmatrix}. \quad (5)$$

The normal $\vec{n} = (n_x, n_y, n_z)$ is calculated from

$$\vec{n} = \frac{\left(-\frac{\partial z}{\partial x}, -\frac{\partial z}{\partial y}, 1\right)}{\sqrt{\left(\frac{\partial z}{\partial x}\right)^2 + \left(\frac{\partial z}{\partial y}\right)^2 + 1}}. \quad (6)$$

To guarantee against errors that would be caused by discontinuities in the range profile, the pixels inside the convolution windows are validated according to some threshold for the departure with central values, and the weight of the operator is adjusted accordingly.

As discussed below, the normal vector $\vec{n}$ serves to calculate the cosine of the reflection angle

$$\cos\theta_o = \vec{\mu}_o \cdot \vec{n} \quad (7)$$

which is used to compensate for foreshortening effects. Errors on $\cos\theta_o$ directly affect reflectance factors measurements. Using (5) and (7) and assuming $\Delta x = \Delta y$, the following expression can be obtained for the relative error on $\cos\theta_o$:

$$\frac{\delta(\cos\theta_o)}{\cos\theta_o} = \frac{\sin\theta_o \cos\theta_o}{\sqrt{6}} \frac{\delta z}{\Delta x} \quad (8)$$

where δz is the expected error on range measurements. This result indicates that high depth accuracy is necessary if reflectance factors are to be computed on a dense sampling grid. For example, in order to keep the error on $\cos\theta_o$ below 2% and assuming $\Delta x = \Delta y = 0.25$ mm, a range accuracy of 25 μm becomes necessary. This corresponds to the level of performance typically achieved with the laser scanner.

B. Radiometric Considerations

Although the position of the imaged spot on the solid-state detector provides the information needed for range measurement, information about reflectance must come from the amplitude of the signal associated with this spot. With the laser scanner, the spot's image extends over a few elements of the CCD linear detector. This condition allows the computation of the spot position to subpixel accuracy using the algorithm described in [5]. Two approaches are possible for connecting the image intensity to object reflectance. Both involve the comparison of the signal from surface elements to that from a white Lambertian surface kept inside the field of view during acquisition.

A first approach is to consider that the signal from each CCD element is a direct measure of the irradiance profile in the imaging plane. Because this profile is itself proportional to the radiance reflected by objects [11], reflectance factors can be obtained by comparing the signal from the target with that from the reference surface, taking into account the cosines of the incidence angles. The difficulty with this approach is that the assumption of a signal proportional to object radiance is valid only if perfect optical resolution is achieved. In practice, CCD elements have finite dimensions, and optical aberrations are present. Additional blurring can result if the electronic signal is filtered to remove unwanted features such as aliasing. Finally, the irradiance provided by the laser is sensitive to the way, it is collimated and can vary with target position. Nevertheless, the whole approach is manageable but requires a sophisticated model for the camera and some calibration procedures. This avenue is perhaps the only one for range finders that work by detecting lines or stripes using 2-D video cameras.

A second approach is to integrate the power collected by the whole CCD. This corresponds to measuring the radiant flux from the flying spot caught by the lens. This quantity varies as the inverse square of the distance ℓ between lens and spot. For a Lambertian surface, it is also proportional to the laser power times the cosine of the reflection angle. Because the lens in Fig. 2 is located at a known small distance from the observation pivot (x_o, z_o), values of ℓ can be recovered for any position (x, y, z) of the spot, and this information can be used to compensate for the effect of distance. The BRDF factor at a sampled point (x, y, z) is then given by

$$R(x, y, z) = \Phi(x, y, z)\left[\frac{\Phi(x_w, y_w, z_w)(\vec{\mu}_o \cdot \vec{n})\ell_w^2}{(\vec{\mu}_{ow} \cdot \vec{n}_w)\ell^2}\right]^{-1} \quad (9)$$

where Φ designates the radiant flux signal and where the subscript w stands for the white Lambertian reference surface. The bracketed term in (9) is simply the radiant flux that would be reflected by a Lambertian surface under equivalent illumination conditions as for the sampled target point.

The surface resolution for BRDF measurement corresponds to the area of the laser spot, which is typically 0.1 mm wide. The angular resolution is fixed by the solid angle covered by the lens, as seen from object plane. At full lens aperture, this is typically 0.001 steradian.

The white standard used as a reference is a flat bar coated with a barium sulphite paint. This material is reported to have very good Lambertian behaviors [3]. The bar is placed in the field of view of the camera to cover a few tens of pixels in all recordings of color and range images. The image of the reference bar also serves to compensate for any drift of the laser power that may occur during image acquisition.

C. Spectral Measurements

The version of the sensor reported here makes use of a He-Cd$^+$ *RGB laser*. This illuminant is a balanced mixture of three wavelengths $\lambda_r = 636$ nm, $\lambda_g = 536$ nm, and $\lambda_b = 442$ nm and appears white. At the present time, each wavelength is isolated using an interference filter, and R, G, and B intensity images are collected separately. The system is currently being modified so these three acquisitions can be done simultaneously.

Color appearance, in connection with a human visual system, is best described in terms of *color tristimulus* X, Y, and Z. These are defined as integrals, which are weighted by *color matching functions* and carried over the whole visible spectrum [12], [16]. The use of only three wavelengths leaves little space for the numerical evaluation of such integrals. Instead, one can refer to the known chromaticities to each wavelength and compute tristimulus using the *center-of-gravity law* of color mixture [16]. This corresponds to measuring the visual

appearance of scenes under white laser illumination. One can gain insight about the quality of the color reproduction obtained this way by considering that the spectrum of the white laser is close to that of a *three-band fluorescent lamp*. This type of lamp is sometimes used in stores to help improve the color appearance of goods. It has a tendency to increase the saturation of most colors [12]. Although it is difficult to quantify, the apparent color differences obtained with the system seem comparable to the ones typically observed in photographic or video reproduction.

Obviously, the color fidelity could be improved by including additional wavelengths. Gaussian quadrature methods are reported for the calculation of tristimulus using as few as seven wavelengths, where some of which have so little weight that they can be omitted with negligible effect on accuracy [16]. Improvements along this line will be eased by the availability of laser diodes covering the visible spectrum.

IV. Reflectance Modeling

The system described in Section III allows the mapping of spectral BRDF factors to surface elements (*surfel*). These factors are, however, sampled for only one particular geometry of the incident and one reflected beam at each surfel. This does not seem to be much information compared with the full expression of BRDF that involves the four independent orientation variables $\theta_i, \phi_i, \theta_o, \phi_o$. The easiest way to recover the full BRDF information is to assume a functional form for it. A given functional form is plausible if it does not violate any known physical laws and if it can be justified by sound assumptions about underlying stochastic processes occurring at the microscopic level. One of the above stated physical laws is the *reciprocity law* [7], in which BRDF expressions should be invariant when orientation variables of the incident and reflected beam are interchanged. This section considers some particular functional forms that respect this condition and are specializations of the dichromatic reflection model (4). It is shown that these can be used to interpret the data collected with the laser range finder. Tasks of increasing complexities are considered, and experimental results accompany the discussion.

A. Lambertian Reflection

The following task, although it is the simplest, perhaps leads to the most useful applications. It consists of measuring the reflectance factor of a Lambertian object, namely, a sphere coated with barium sulphite paint, which is the very same substance used for the white reference standard discussed in Section III-B.

In this case, the following functional form is assumed for the dichromatic model (4):

- $m_b() = 1$
- $c_b(\lambda) = R_b$
- $c_s(\lambda) = 0$

where R_b is the *reflectance* of the coating.

Experimentation was done using a 60-mm-in-diameter sphere $\sim$, which was sampled at the blue wavelength at 0.25–mm intervals in both the x and y directions. A consistent value $R = 1.03 \pm 0.03$ was obtained for all the surface elements, with the exception of those for which the reflection angle exceeded $\sim 70°$.

This case is important because many matte nonwhite objects can be approximated according to the same model, with $R_b(\lambda)$ allowed to take values between 0 and 1. Even glossy surfaces can be tilted to eliminate surface reflections. In these cases, the mapping of body reflectance factors to surface elements is not limited by the restrictive assumption that the scene should have uniform material composition.

A. Reflection by a Rough Surface

A geometric approach to the problem of reflection by rough surfaces was proposed by Torrance and Sparrow [25] in 1967. They considered a rough surface as a collection of mirror-like micro facets oriented at random according to some Gaussian probability distribution. With this model, the amount of energy transferred from an incoming direction $\vec{\mu}_i$ to an outgoing direction $\vec{\mu}_o$ is proportional to the number of facets that have their normals $\vec{n}'$ in the $(\vec{\mu}_i + \vec{\mu}_o)/2$ direction. Additional terms can also account for masking, shadowing, and diffuse reflection from multiple reflections occurring at the microscale. This model has been used in computer graphics to generate synthesized images of highly realistic metallic surfaces [8].

The original paper by Torrance and Sparrow reports a form for BRDF that has been normalized with respect to that in the specular direction. Unfortunately, this eliminates some multiplicative factors that are important for absolute measurements. If the unnormalized Gaussian distribution for facet orientations, as proposed by Torrance-Sparrow, is replaced by a distribution that is normalized to 1 with respect to all possible orientations, the following expression for the BRDF factor R can be obtained:

$$R = gF(\lambda) + (1-g)\frac{F(\lambda)\, e^{-\frac{1-(\vec{n}'\cdot\vec{n})^2}{2\sigma^2(\vec{n}'\cdot\vec{n})^2}}}{8\sigma^2(\vec{\mu}_i\cdot\vec{n})(\vec{\mu}_o\cdot\vec{n})(\vec{n}'\cdot\vec{n})^4}, \tag{10}$$

where $\vec{n}'$ is the unit vector corresponding to the normal of those facets that reflect specularly toward the observer:

$$\vec{n}' = \frac{\vec{\mu}_i + \vec{\mu}_o}{\|\vec{\mu}_i + \vec{\mu}_o\|} \tag{11}$$

where $F(\lambda)$ is the Fresnel reflectance of the surface, and σ is its RMS *slope surface roughness* [2], [3]. The factor g represents the fraction of energy that is diffusely scattered from multiple reflections involving two or more microfacets.

The model applies to metallic surfaces, for which reflection occurs essentially at the outer surface level. It is a specialization of the dichromatic model with

- $c_b(\lambda) = 0$
- $c_s(\lambda) = F(\lambda)$
- $m_s() = g + (1-g)\frac{e^{\frac{-1-(\vec{n}'\cdot\vec{n})^2}{2\sigma^2(\vec{n}'\cdot\vec{n})^2}}}{8\sigma^2(\vec{\mu}_i\cdot\vec{n})(\vec{\mu}_o\cdot\vec{n})(\vec{n}'\cdot\vec{n})^4}$.

This model was tested using a sand-blasted steel ball bearing as a target. This object is 25.4 mm in diameter and has a grey pearl appearance. It was sampled with the scanner at 0.25-mm intervals in both the x and y directions. Fig. 3(a) shows the BRDF factors sampled at the blue wavelength. Again, undersampling at 1-mm intervals is used to ease the graphical presentation. These data were fitted to (10) using a library routine, namely, the *Lavenberg-Marquardt* method. [17]. The orientation vectors in (10) are the independent variables, and F, σ, g are the free parameters that are adjusted to minimize the χ^2 merit function. The values obtained for the parameters are listed in Table I. These can be fed back in (10) to produce a synthesized reflectance image of the ball (Fig. 3). The goodness of fit can be judged by comparing Fig. 3(a) and (b).

Fresnel reflectance is usually a function of the incidence angle. With the laser scanner, because only facets with their normals along $\vec{n}'$ participate in directing reflections toward the detector, the factor $F(\lambda)$ involved in (10) applies essentially for incidence angles equal to $\gamma/2$ (Fig. 2), irrespective of the orientation $\vec{n}$ of the mean macroscopic surface. The autosynchronization of the scanner keeps γ almost constant. With $\gamma \sim 10°$ and according to the fact that $F(\lambda)$ varies slowly with incidence angle for most materials, the value of $F(\lambda)$ obtained with the method can be considered to be approximately equal to the Fresnel reflectance for normal incidence.

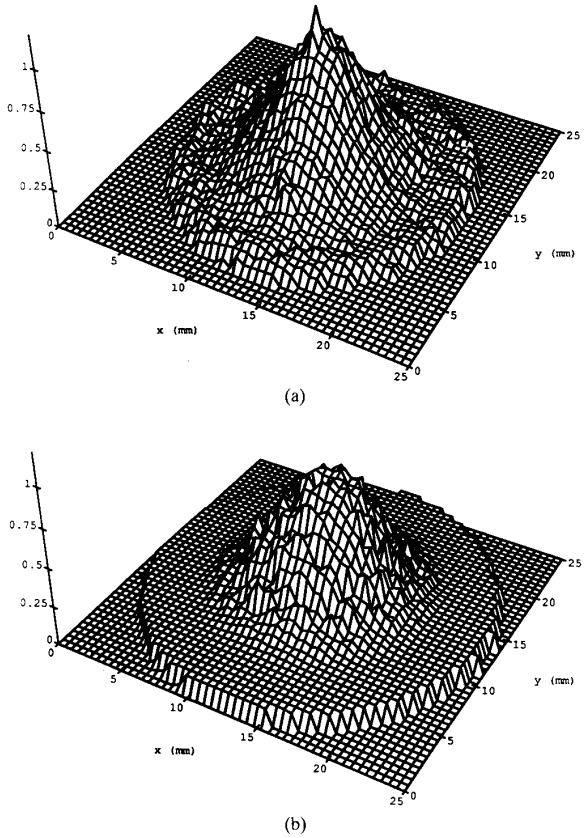

Fig. 3. (a) Reflectance image of a roughened steel ball; (b) reflectance image as synthesized using the parameters extracted with the least-squares routine.

To assess the value $F = 0.43$ obtained with this method, the Fresnel reflectance of the material was measured independently on a nonsand-blasted ball bearing. Because it is very shiny, the Fresnel reflectance of a brand new bearing is easily measured using the laser and a power meter. The value obtained with this method is $F = 0.44$.

C. Mixed Body and Surface Reflection

This case is a combination of the last two. Many reflecting materials consist of tiny particles, such as pigments and lacquers, imbedded in an otherwise homogeneous vehicle such as acrylic or oil. The particles selectively absorb and scatter the light, depending on wavelength, and are mostly responsible for color appearance. This form of diffuse reflection that occurs inside of the material is called *body reflection* and is well approximated by the Lambertian model. The vehicle itself only reflects light at the air-vehicle interface, and the fraction of energy involved is the Fresnel reflectance of this vehicle. This form of reflection is called *surface reflection* [14], although other terms such as *interface reflection* [23] and *neutral interface reflection* [15] are also used to designate the same phenomenon. Typically, only a small percentage of the energy is reflected at the interface but, because surface reflection is highly directional, it can constitute a large fraction of the total energy reflected in the specular direction. If the air-vehicle interface is rough, the Torrance-Sparrow model can be used to formulate the surface reflection. All these considerations lead to the following specialization of the dichromatic reflection model:

TABLE I
REFLECTANCE PARAMETERS MEASURED FOR DIFFERENT OBJECTS

Object	λ	R_b	F	σ	g
Lambertian ball	blue	1.03			
Steel ball	blue		0.43	0.233	0.26
Painted ball	blue	0.222	0.0217	0.202	
Pencil 1	red	0.760	0.015	0.127	
	green	0.664	0.015	0.116	
	blue	0.292	0.016	0.114	
Pencil 2	red	0.038	0.014	0.156	
	green	0.220	0.014	0.150	
	blue	0.350	0.014	0.142	
Pencil 3	red	0.205	0.010	0.134	
	green	0.222	0.011	0.135	
	blue	0.252	0.011	0.133	

- $m_b() = 1$
- $c_b(\lambda) = R_b(\lambda)$
- $m_s() = \frac{e^{-\frac{1-(\vec{n}'\cdot\vec{n})^2}{2\sigma^2(\vec{n}'\cdot\vec{n})^2}}}{8\sigma^2(\vec{\mu}_i\cdot\vec{n})(\vec{\mu}_o\cdot\vec{n})(\vec{n}'\cdot\vec{n})^4}$
- $c_s(\lambda) = F(\lambda)$.

The energy that is diffusely scattered by the rough surface, through multiple reflections among the facets, cannot be distinguished from that diffusely reflected from the body. Section IV-B showed that the corresponding fraction g was indeed small, even for a very rough surface, and g can be neglected without inducing much error.

This model was tested on a sphere coated with a uniform layer of a grey-colored commercial spray paint. Results for the parameters R_b, F, σ, which are recovered through least-squares fit, are listed in Table I. F and σ were used, along with the range data, to synthesize the image that corresponds to surface reflection alone (Fig. 4(a)). By subtracting this image from the sensed reflectance image, a new image is obtained that corresponds to body reflection alone (Fig. 4(b)). In this case, a consistent value $R_b = 0.223 \pm 0.01$ was obtained even for large incidence-reflection angles.

Many colored objects can be expected to be uniform in their F and σ values. This could be the case with an artist's painting protected by a varnish layer. If F and σ can be established by working on a small portion that is also uniform in R_b, then a device-independent description of each surfel can be recorded with the scanner. This idea is discussed further in the next section.

D. Color Modeling

This section adds the dimension of color to data modeling. With the availability of multispectral reflectance information, not only can the preceding methods be applied independently at each wavelength, but the color-space information can also be used to lessen the constraints about the uniformity of the scene composition.

The reflection models presented above are here applied to the color and range image of color drawing pencils represented in the top of Fig. 5. This stereo pair was obtained by mapping the sensed R, G, and B intensities on the form synthesized from the range data. Because the simulated point of view differs from that of the sensor—the camera head was on top of the scene for the recording—the relative positions of the shading and highlight patterns appear unnatural in this representation.

The aim of the experiment is to classify each surfel according to its belonging to a particular pencil. Here, the question of the exactitude of color measurement, relative to the human visual system, is irrelevant.

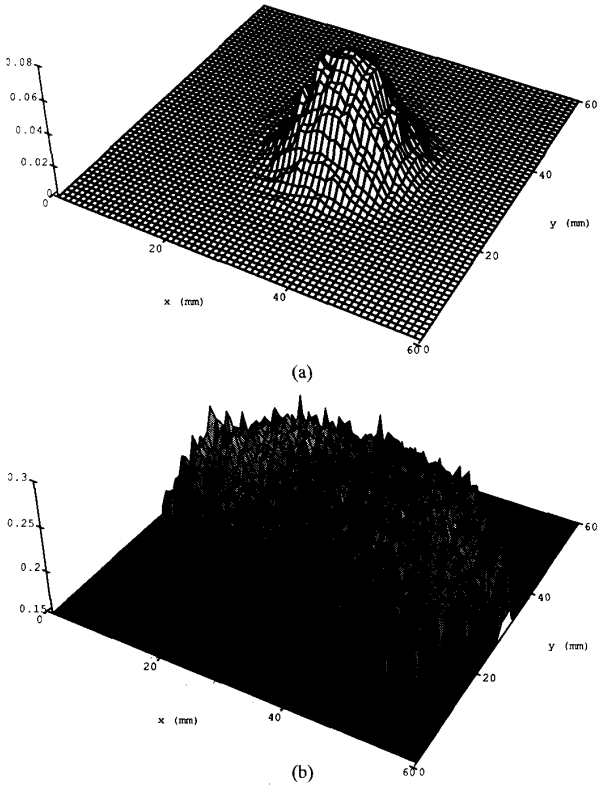

Fig. 4. (a) Surface reflectance image and (b) body reflectance image of a ball coated with a commercial grey paint.

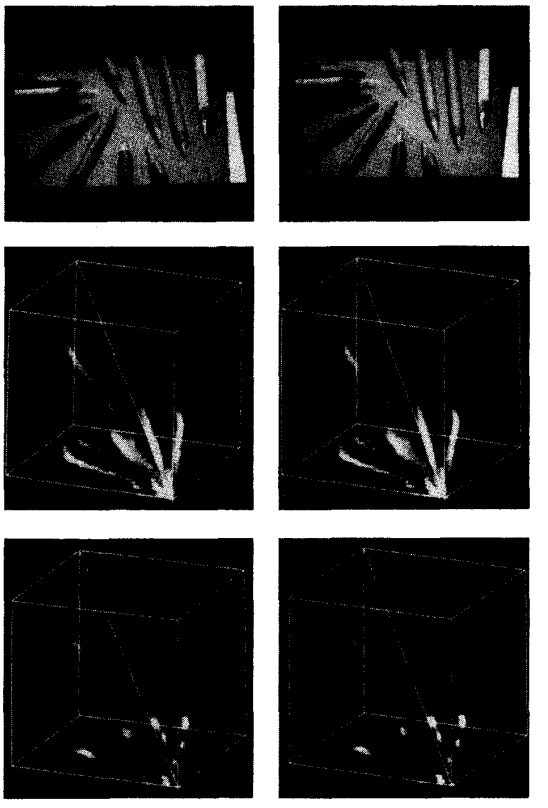

Fig. 5. Experimental results displayed as stereo pairs. The top image is a computer-generated stereo pair of the registered color and range image. The center pair shows the histogram of the red, green, and blue values (density expressed as grey level) in the color cube. The bottom pair shows the histogram of the recovered body reflectance factors in the same color cube.

In this example, classification of surface elements based on the *saturation* of colors would be fooled by highlights. A classification based on *hue* would also fail if two pencils happened to have the same hue but differed only in their *lightness*. A classification based on hue *and* lightness would be affected by the orientation of the surfels. This observation holds for any transformation of the 3-D color space into one or two dimensions that would attempt to compensate for the changes in lightness caused by varying surface orientations. It thus appears that the dimensionality of the color space should be kept to three. In fact, more wavelengths might be needed to resolve possible coincidence of reflectance by two different materials.

The center of Fig. 5 shows, as a stereo-pair 3-D histogram, the distribution of raw intensity data prior to any processing. The axes of the cube are the red, green, and blue wavelengths. Here, the histogram contributions of the background plane and the calibration white bar have been removed to enhance the visibility of the pencil color clusters. This was done in a straightforward manner, using thresholding based on the range data.

Using the terminology of Klinker [14], pixels corresponding to a particular pencil distribute into a cluster that has a *skewed L* shape. One branch of the L (the *matte line*) points toward the origin of the cube and is due mostly to the foreshortening effect on diffuse reflection. The other branch (the *highlight line*) is directed toward the color of the white laser and is due to surface reflection.

To analyze the color image, the spectral BRDF factors were first established using the method of Section III. Three different pencils were then isolated from the whole image, and the factors $R_b(\lambda), F(\lambda), \sigma$ were evaluated for each of them and for each of the three colors using the method of Section IV-C. The values obtained are shown in Table I. As expected, $F(\lambda)$ is seen to be only slightly affected by color, and σ does not vary much from one pencil to the other. Average values for $F(\lambda)$ and σ were used to synthesize the surface reflection components, which were then subtracted from each of the color reflectance images. The bottom of Fig. 5 shows the color histogram of the resulting reflectance image. Clusters have been reduced to compact ones, and each of these corresponds to one pencil. The histogram immediately indicates how many distinct body materials are in the scene and what their color is. This histogram is a sort of *color space signature* of the scene.

The fact that some pencils had to be isolated for parameter recovery seems somewhat restrictive in this example. A more clever usage of color histograms can help to automatize the process and lessen the constraints about the uniformity of σ and F. Klinker *et al.* [13] have suggested an interesting method to deal with this sort of histogram. They generate and exploit geometric hypothesis about the shape of a cluster to grow regions in the scene that correspond to material composition. A similar approach can be used in the case of color-and-range images. For example, if each of the pencils had different sets of parameters $R_b(\lambda), F(\lambda), \sigma$, the color histogram corresponding to intensity would still show some skewed L clusters. After performing the reflectance factor recovery using the range data, the matte lines would shrink to point-like clusters, from which would originate the highlight lines. These *comet* shaped clusters could be recognized and

serve for the classification of surfels. Each type of surfel would then be fed in turn to the least-squares fit routine for the recovery of the intrinsic reflectance parameters corresponding to each class.

V. Conclusion

This paper describes a sensing device for range and color acquisition. It is shown that the explicit shape information provided by the 3-D data allows the interpretation of the registered intensity data in terms of the underlying physical reflectance properties of the scene. This facilitates the task of color image understanding. By resorting to a careful modeling of the geometrical and optical properties of the camera, the sensor can, in fact, be turned into a precise analytic instrument.

The system described is specially suited for the extraction of intrinsic object properties in connection with appropriate physical models. The ones considered here involve the body reflectance, Fresnel reflectance, and slope surface roughness of the sampled surface elements. Although they make simplifying assumptions, they nevertheless fit the data very well. More elaborate models, such as those described in Beckmann- Spizzichino [2] and Egan-Hilgeman [9], could be used in connection with the same system.

Potential applications of the system presented in the paper are in art conservation, datagraphy (electronic museum) [21], object modeling for computer-assisted design and graphics, robot vision, and, more generally, in 3-D scene understanding.

VI. Acknowledgments

The authors wish to thank L. Cournoyer from the Institute for Information Technology of the National Research Council of Canada, for his help in building the prototype of the color/range sensor and in image acquisition, and C. X. Dodd from the Institute for National Measurements Standards of the NRCC, for his assistance in the fabrication of the white reflectance standard.

References

[1] R. Baribeau and M. Rioux, "Influence of speckle on laser range finders," *Appl. Optics*, vol. 30, no. 20, pp. 2873–2878, 1991.
[2] P. Beckmann and A. Spizzichino, *The Scattering of Electromagnetic Waves from Rough Surfaces*. New York: Artech, 1987.
[3] J. M. Bennett and L. Mattsson, *Introduction to Surface Roughness and Scattering*. Washington, DC: Opt. Soc. Amer., 1989.
[4] P. J. Besl, "Active, optical range imaging sensors," *Machine Vision Applications*, vol. 1, no. 2, pp. 127–152, 1988.
[5] F. Blais and M. Rioux, "Real-time numerical peak detector," *Signal Processing*, vol. 11, pp. 145–155, 1986.
[6] P. Boulanger, M. Rioux, J. Taylor, and F. Livingstone, "Automatic replication and recording of museum artifacts," in *Proc. 12th Int. Symp. Cons. Rest. Cultural Property,* (Tokyo), 1988, pp.131–147.
[7] S. Chandrasekhar, *Radiative Transfer*. New York: Dover, 1960.
[8] R. L. Cook and K. E. Torrance, "A reflectance model for computer graphics," *ACM Trans. Graphics*, vol. 1, no. 1, pp. 7–24, 1982.
[9] W. Egan and T. Hilgeman, *Optical Properties of Inhomogeneous Materials*. New York: Academic, 1975.
[10] G. Healey, "Using color for geometry-insensitive segmentation," *J. Opt. Soc. Amer. A,* vol. 6, no. 6, pp. 920–937, June 1989.
[11] B. K. P. Horn, *Robot Vision*. Cambridge, MA: MIT Press, 1986.
[12] R. W. G. Hunt, *Measuring Color*. New York: Wiley, 1987.
[13] G. J. Klinker, "A physical approach to color image understanding," Ph. D. thesis, Carnegie Mellon Univ., Pittsburgh, PA, 1988.
[14] G. J. Klinker, S. A. Shafer, and T. Kanade, "A physical approach to color image understanding," *Int. J. Comput. Vision*, vol. 4, pp. 7–38, 1990.
[15] H. Lee, E. J. Breneman, and C. P. Schulte, "Modeling light reflection for computer color vision," *IEEE Trans. Patt. Anal. Machine Intell.*, vol. 12, no. 4, pp. 402–409, 1990.
[16] D. L. MacAdam, *Color Measurement*. New York: Springer-Verlag, 1981.
[17] D. W. Marquardt, *J. Soc. Ind. Appl. Math.*, vol. 11, pp. 431–441.
[18] S. K. Nayar, K. Ikeuchi, and T. Kanade, "Extracting shape and reflectance properties of Lambertian, specular, and hybrid surfaces," Report CMU-RI-TR-88–14, Carnegie Mellon Univ., Pittsburgh, PA, 1988.
[19] F. E. Nicodemus, J. C. Richmond, J. J. Hsia, I. W. Ginsberg and T. Limperis, "Geometrical considerations and nomenclature for reflectance," NBS Monograph 160, Nat. Bureau Standards, Washington, DC, Oct. 1977.
[20] M. Rioux, "Laser range finder based on synchronized scanners," *Appl. Optics*, vol. 23, no. 21, Nov. 1984.
[21] ——, "Computer acquisition and display of 3-D objects using a synchronized laser scanner," in *Proc. 1989 Int. Conf. Three Dimensional Media Technology,* (Montreal), May 1989, pp. 253–268.
[22] M. Rioux, F. Blais, J. -A. Beraldin, P. Boulanger, "Range imaging sensors development at NRC laboratories," in *Proc. IEEE Comput. Soc. Workshop Interpretation 3D Scenes* (Austin, TX), Nov. 27–29, 1989.
[23] S. Shafer, "Using color to separate reflection components," *COLOR Res. Applications,* vol. 10, no. 4, pp. 210–218, 1985.
[24] H. D. Tagare and R. J. P. deFigueiredo, "A theory of photometric stereo for a class of diffuse non-Lambertian Surfaces," *IEEE Trans. Patt. Anal. Machine Intell.,* vol. 13, no. 2, pp. 133–152, 1991.
[25] K. E. Torrance and E. M. Sparrow, "Theory of off-specular reflection from roughened surfaces," *J. Opt. Soc. Amer.*, vol. 57, pp. 1105–1114, 1967.
[26] R. J. Woodham, "Photometric method for determining surface orientation from multiple images," in *Shape From Shading* (B. K. P. Horn and M. J. Brooks, Eds.). Cambridge, MA: MIT Press, 1989.

Using Models to Improve Stereo Reconstruction

Henri Maître and Wei Luo

***Abstract*—We propose the collaboration of photometric and stereometric information to solve the stereo vision problem in the case of man-made environment. The proposed method improves a) the accuracy of the stereo information and b) its density by introducing a hypothesis on the object surfaces. Two kinds of hypotheses have been developed here: planar and quadratic objects. Reconstructions of complex scenes are given.**

***Index Terms*—Cooperation between photometry and stereo, stereovision, 3-D models.**

I. Introduction

It has been demonstrated by Julesz that the perception of the 3-D structure of our environment by means of our visual system may be obtained before the monocular interpretation of the scene. From this starting point, several methods have been proposed to solve the automatic stereovision problem, which is essentially based on the detection of features, followed by a matching procedure. Good results can be obtained every time the observed image is richly textured. In contrast, all existing methods usually fail in cases with abrupt depth changes separated by poorly textured regions or if hidden parts and major appearance differences occur due to parallax or shadings.

Manuscript received October 1, 1990; revised February 26, 1991.
The authors are with Département Images, Telecom Paris, Paris, France.
IEEE Log Number 9102689.